MANSOURA JOURNAL OF CHEMISTRY
Official Journal of Faculty of Science, Mansoura University, Egypt
E-mail: scimag@mans.edu.eg ISSN: 1687-5060

Characterization and Spectroscopic characteristics of chitosan poly ethylene oxide (Cs/PEO) polymer blends

***Ch. Wahid*[a]*, *A.M. Abdelghany*[b], *D.M. Ayad*[a], *Weam M. Abou El-maaty*[a]**

[a]*Chemistry Department, Faculty of Science, Mansoura University, Mansoura, 35516, Egypt*
[b]*Spectroscopy Department, Physics Research Institute, National Research Center, 33 Elbehouth St., 12311, Dokki, Giza, Egypt*
Corresponding Author: *Ch. Wahid; E-mail: christen.wahid@gmail.com,Tel.01204002851*

Received:27/3/2023
Accepted: 11/4/2023

Abstract: Thin films comprising different mass fractions of chitosan/polyethylene oxide (Cs/PEO) were successfully synthesized via ordinary solution casting technique. Synthesized thin films characterized in terms of chitosan content using x-ray diffraction (XRD), Fourier transforms infrared (FT-IR), and scanning electron microscopy (SEM) adopted to study surface morphology. Synthesized membranes exhibit a higher degree of crystallinity, according to XRD data decreases with increasing chitosan content. Infrared spectroscopy revealed that the studied samples show significant structural changes as a result of intermolecular interactions with the appearance of characteristic peaks belonging to individual polymers. The change in intensity may be attributed to the molecular interaction through strong hydrogen bonds between hydroxyl and amino groups on chitosan molecules and ether groups in PEO. Roughness parameters appear to be correlated with the increase in chitosan content.

keywords: PEO/Cs; XRD; FTIR; Roughness parameters

1.Introduction

Polymer blending attracts the curiosity of several scientists within the last decades because of their superior characteristics among their separate polymer networks and wide applications [1-3].

The characteristics of poly (ethylene oxide) include a moderate tensile modulus, high elongation, and the capacity to orient under stress. Its molecular weight and temperature affect its solubility in various solvents. PEO with a larger molecular weight is typically more difficult to dissolve. PEO is used in adhesives and the defense against fire in the industry [4, 5].

Chitosan is a positively charged natural polysaccharide, which is composed of β-(1→4)-linked N-acetyl-D-glucosamine (GlcNAc) and D-glucosamine (GlcN) [6]. Chitosan is a non-toxic, cost-effective, renewable, biodegradable, and environmentally friendly material [7]. Chitosan is derived from the deacetylation of chitin polymer, and it is soluble in acidic aqueous media because of the existence of amino groups Chitosan has a high ability to form films, but biopolymers are more expensive than synthetic polymers. So, to overcome that, blending between natural and synthetic polymers introduces new substances with improved characteristics with reduced costs [8]. chitosan exhibits antimicrobial activity only in an acidic medium [9, 10]. Several factors influence chitosan's antibacterial activity, including the type of chitosan, the degree of chitosan polymerization, and some of its other physicochemical properties. Chitosan is more effective against Gram-positive bacteria than Gram-negative bacteria. Chitosan's antibacterial activity is also affected by its molecular weight and solvent [11], and it is inversely affected by pH, with higher activity at lower pH values [12]. Wide-ranging biomedical uses of chitosan include drug delivery systems [13], charcoal-encapsulated chitosan beads for toxin elimination [4], dental and orthopedic materials [15, 16], and more. Its biodegradable, nontoxic, and biocompatible properties are chiefly to blame for this [17]. Fibers for fat blockers, digestible sutures, liposome stability,

antibacterial, antiviral, and antitumor medicines, as well as hemostatic and hypocholesterolemic, and hypolipidemic agents, are further applications in the biomedical sector [18].

Chitosan has great mechanical strength, is permeable to urea, amino acids, and creatinine, and can reject substances with high molecular weights. Because it is impervious to serum proteins, harmful metals may not enter the bloodstream [19, 20]. Mallete et al. [21] showed that the hemostatic activity of chitosan solution entailed the agglutination of red blood cells and that it generated a coagulum whenever in contact with blood.

Electrospun chitosan/PEO nanofibres have been used to adsorb heavy metals such as copper, lead, cadmium, and nickel ions from an aqueous solution [22, 23]. Blending natural and synthetic polymers opens up the prospect of developing new materials, as films generated by combining two or more polymers often have different physical and mechanical properties than films made from individual components.

Presented work intended to characterize and correlate the physicochemical characteristics of chitosan containing different mass fractions PEO with the composition and surface morphology of the studied membranes.

2. Materials and methods

Chitosan (Cs) polymer of chemical formula [($C_6H_{13}NO_5$) and high molecular weight] was obtained from (Aldrich Co.). Polyethylene oxide (PEO) of molecular weight 140,000 was supplied by Alpha Acer Company. The chemical structure of both polymers is shown in Figure (1).

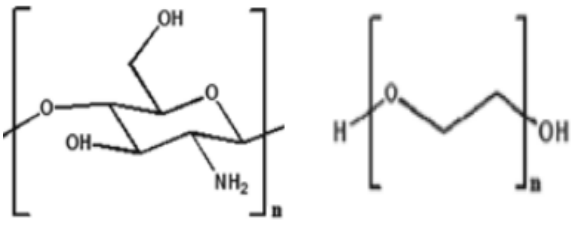

Cs **PEO**

Figure (1) Chemical structure of both Cs and PEO polymers

Precalculated amounts of both Cs and PEO with different mass fractions listed in the table (1) chitosan was dissolved separately in a slightly acidic aqueous solution of acetic acid while PEO was dissolved in a double distilled water using a magnetic stirrer. Obtained viscous solutions with proper concentrations were then mixed vigorously and kept at ambient room temperature for about 48h. Clear and bubble-free polymer blend solution was used for the preparation of the blend films. A constant volume of the obtained solution each time was poured into plastic Petri dishes each to ensure the formation of nearly the same thickness films. The dishes were then placed in an incubator regulated at about 50 °C for 24 h. The films were then peeled from the dishes and stored in a dry place until use.

Table (1) Samples nomination and composition.

Sample	Cs	PEO
Cs	100	0
PEO	0	100
Cs30	30	70
Cs40	40	60
Cs50	50	50
Cs60	60	40
Cs70	70	30

2.1 Sample Characterization

X-ray diffraction data (XRD) analyzed by (PAN analytical X' Pert PRO) utilizing CuKα line (λ=1.540 Å) with a tube operating at 30 kV voltage. Bragg's angle (2θ) extended from (5 to 70°) at STP, and the diameter of the incident beam can reach 100μm was used to identify the crystalline/amorphous forms of the samples. Nicolet is10 – Thermo Fischer USA single beam spectrophotometer was used to record the spectral data within the range 4000-400 cm^{-1}. The shape and surface morphology of the studied samples were examined using scanning electron microscopy (SEM) Model SEM-Quanta 600 FEG 2100 JEOL, Japan.

3. Results and Discussion

3.1. X-ray diffraction analysis

Figure (2) reveals the XRD diffraction pattern of synthesized (Cs/PEO) samples with a variable mass fraction polymer blend. Obtained patterns of both virgin polymers and other samples of Cs/PEO blend containing variable mass fractions show their characteristic patterns. XRD pattern of PEO shows two prominent peaks originally located at 21.8° and

17.7° correlated to (1 1 2) and (1 2 0) planes. These easily identifiable diffraction peaks are a reflection of the crystalline or semi-crystalline structure of PEO polymers [24, 25]. Chemical and electrochemical stabilization of the PEO polymer's crystalline structure is the responsibility of structural elements such as the PEO's C-H, C-C, and C-O bonds. While of Chitosan is characterized by a broad hump originally located at about 20° points to the amorphous nature of the studied sample.

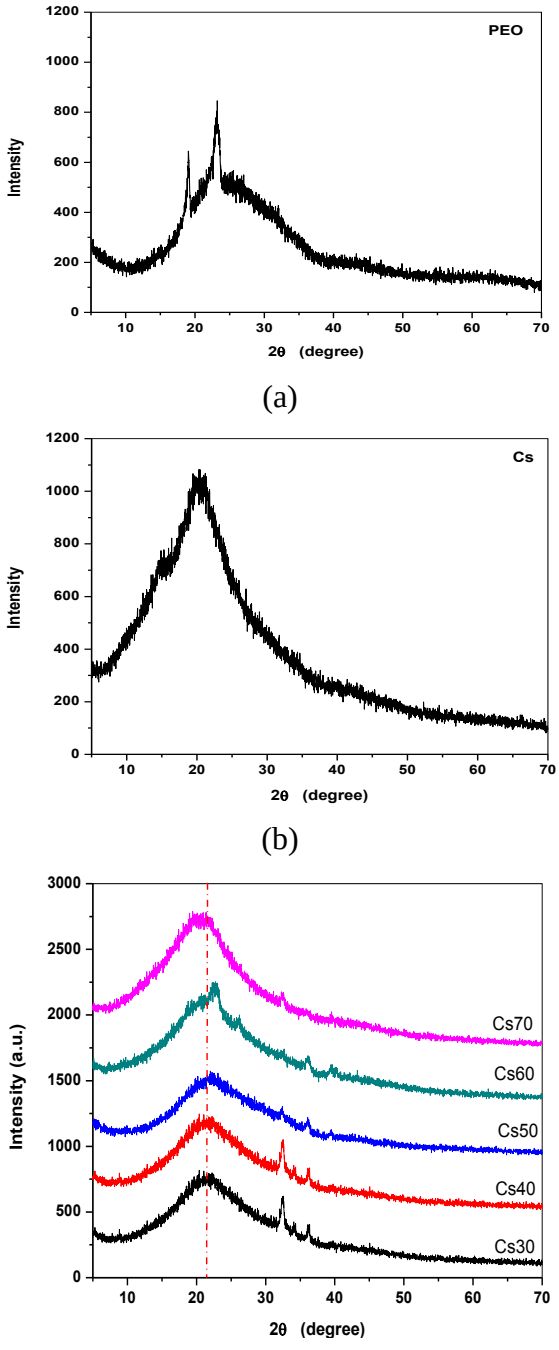

Figure (2) XRD pattern of (a) virgin PEO, (b) Virgin Chitosan, and (c) samples of polymer blends

A decrease in the main broad peak indicates an increase in the amorphous nature of blend films and points to the interaction and crosslinking of the two polymers [26]. An observed shift towards the left with increasing chitosan content with increasing the amorphous nature of the studied samples was also predicted and observed in the pattern. The degree of the crystallinity of studied samples appears to be reduced with increasing chitosan content and is attributed to the increasing entropy of the structure [27].

Figure (3) shows the change in crystallinity with a change in the chitosan content. An increase in the chitosan amorphous phase combined with a decrease in PEO semi-crystalline polymer was followed by a decrease in the crystalline nature of the studied thin films.

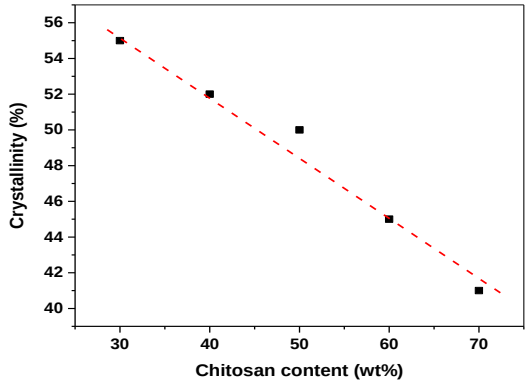

Figure (3) the change in crystallinity with a change in the chitosan content.

Figure (4) reveals the supposed reaction mechanism between both polymers as reported by Pakravan et al [28]. The interaction reveals strong hydrogen bonds between hydroxyl and amino groups on chitosan molecules and ether groups in PEO.

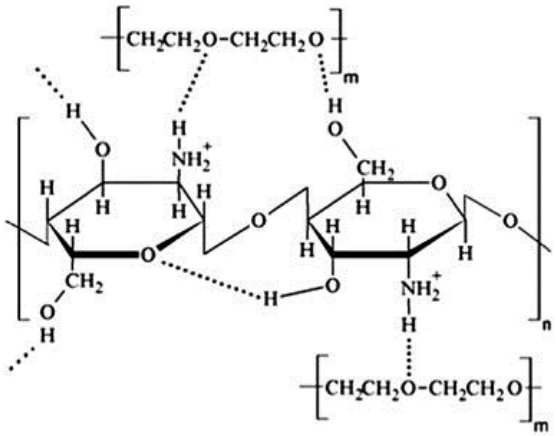

Figure (4) reaction mechanism between both PEO and Chitosan

3.2. FT-IR spectral data

Figure (5) reveals the FT-IR spectra of CS, PEO, and CS/PEO blend samples. CS spectrum contains a broad absorption band at 3372 cm^{-1} related to O-H stretching vibrations, while -CH_2 and -CH_3 groups show stretching vibrations at 2923 and 2878 cm^{-1}, respectively. The N-H groups of CS have an absorption band in the range of 3400-3500 cm^{-1} overlapped with the absorption band of O-H groups [29]. The band at 1639 and 1560 cm^{-1} are related to the vibration of C=O of the amide group CONHR (amide I) and the protonated amine group (amide II), respectively. The peaks at 1410 and 1312 cm^{-1} are corresponding to C-N axial stretching and bending vibrations of O-H and C-H groups. The asymmetric stretching of the C-O-C bridge appears at 1154 cm^{-1}. The saccharide structure of CS has a characteristic absorption band at 1079, 1035, and 657 cm^{-1} [30].

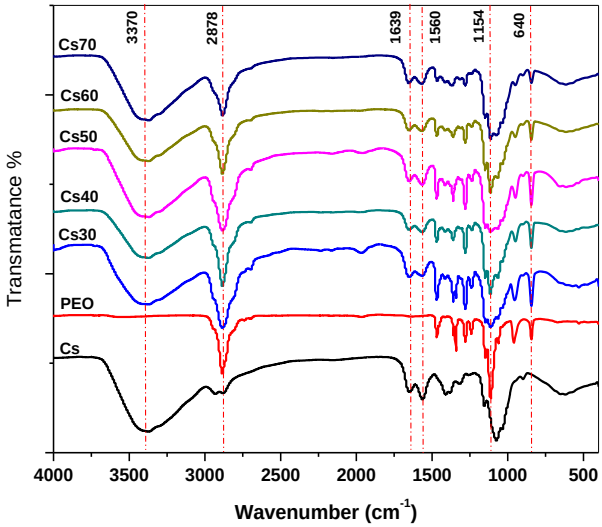

Figure (5) the FT-IR spectra of CS, PEO, and CS/PEO blend samples**.**

PEO spectral data reveals the appearance of three peaks originally located at 1143, 1096, and 1068 cm^{-1} attributed to C–O–C stretching vibrations. The bands located at about 1347 and 1413 cm^{-1} may be correlated to the wagging vibration of CH2 [31]. The peaks at 2862 and 2700 cm^{-1} may be assigned for the asymmetric and symmetric stretching CH2 vibrations, while the peaks at 1280 and 1240 cm^{-1} are correlated with the CH2 asymmetric and symmetric twisting vibrations. The peak at 956 cm^{-1} is assigned to the bending vibration of CH groups, while the peak at 840 cm^{-1} is ascribed to CH2 rocking [32]. Obtained data can be summarized as shown in Table (2).

Table 2: FT-IR spectral data and their assignment for Cs and PEO

	ν (cm^{-1})	**Assignment**
Cs	3372	O-H overlap with N-H stretching
	2923, 2878	C-H symmetric and anti-symmetric stretching
	1639	-C=O stretching
	1560	N-H of the secondary amide stretching
	1410, 1312	C-N axial stretching or O-H and C-H bend vibration
	1154	Asymmetric stretching of the C-O-C bridge
	1079, 1035, 657	stretching of C-O and specific to saccharide structure stretching
PEO	3446	OH stretching
	2862. 2700	CH_2 asymmetric and symmetric stretching
	1662	C=O symmetric stretching
	1443, 1096, 1068	C-O-C stretching vibrations
	1348, 1462	Waggig vibration of CH2
	966	bending vibration of CH
	840	CH2 rocking

FTIR spectral data of the obtained polymer blend appears as a collective sum of the spectra of both individual polymers considering the mechanism of interaction between such polymers. According to such interactions, Figure (6) reveals the suggested reaction model in combination with their HUMO and LUMO energies.

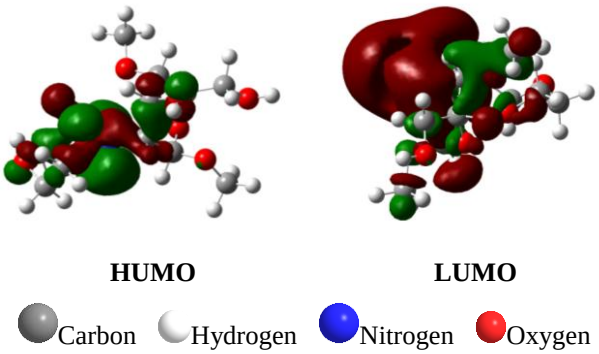

Figure (6) reaction model in combination with their HUMO, LUMO energies

3.3. SEM morphological and surface roughness studies

The surface of the studied thin films was observed by SEM after coating them with a gold thin film. Figure (7) reveals SEM image and their corresponding 3-dimensional (3D) images that may be used to calculate the roughness parameters. SEM images of the selected thin films were used to calculate the

surface roughness parameters of the samples which are summarized in Table 3. Three-dimensional images can be used to estimate the roughness parameters including average roughness (R_a), root mean square roughness (R_q), the maximum height of the roughness (R_t), maximum roughness valley depth (R_v), maximum roughness peak height (R_p), the average maximum height of the roughness (R_{tm}), Such measured parameters specify and support the suitability of the studied sample for specific applications

Table (3) calculated roughness parameters of the studied samples

Roughness Parameter (nm)	CS	PEO	Cs30	Cs40	Cs50	Cs60	Cs70
Ra	25.1832	31.8609	56.1063	32.8421	33.5793	29.9401	31.8982
Rq	31.9324	40.1333	69.0507	40.6605	41.9519	37.4474	40.0849
Rt	233.224	257.838	411.102	240.8	264.506	249.042	261.288
Rv	92.2555	125.509	202.582	105.121	111.653	136.121	123.462
Rp	140.969	132.329	208.52	135.679	152.852	112.921	137.826
Rtm	189.187	236.711	367.217	215.981	240.749	211.093	231.535
Rvm	85.7358	113.338	176.999	98.4673	101.496	104.458	114.407
Rpm	103.451	123.373	190.218	117.513	139.253	106.635	117.128
R3z	196.451	242.213	380.845	223.616	248.807	208.914	232.763
R3z ISO	153.779	189.735	298.476	185.749	188.327	175.442	191.507
Rz	196.061	243.08	378.828	224.973	245.899	218.467	236.479
Rz ISO	189.187	236.711	367.217	215.981	240.749	211.093	231.535
Ry = Rmax	222.481	255.203	411.102	233.224	252.813	248.018	261.288
Rsk	0.20369	0.1161	0.11263	0.23864	0.36991	0.056623	0.08643
Rku	3.22897	3.11813	2.70967	2.8209	3.06051	2.98082	3.02035
Wa	10.0567	18.7075	43.1967	11.2793	18.0721	14.5575	12.2202
Wq	13.9502	24.8869	53.5246	14.5966	21.6142	19.9562	16.2109
Wy = Wmax	86.1031	154.965	297.607	84.6934	120.425	140.818	117.757
Pt	239.202	284.616	510.536	273.917	293.914	306.631	259.928

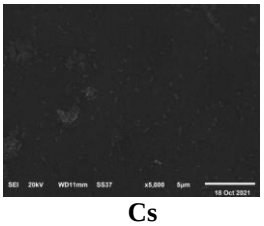

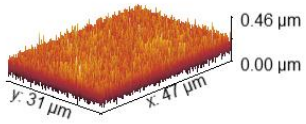

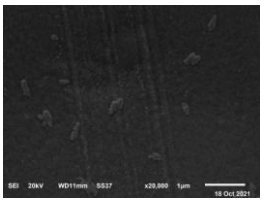

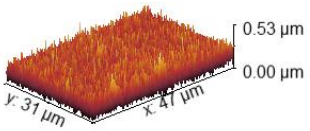

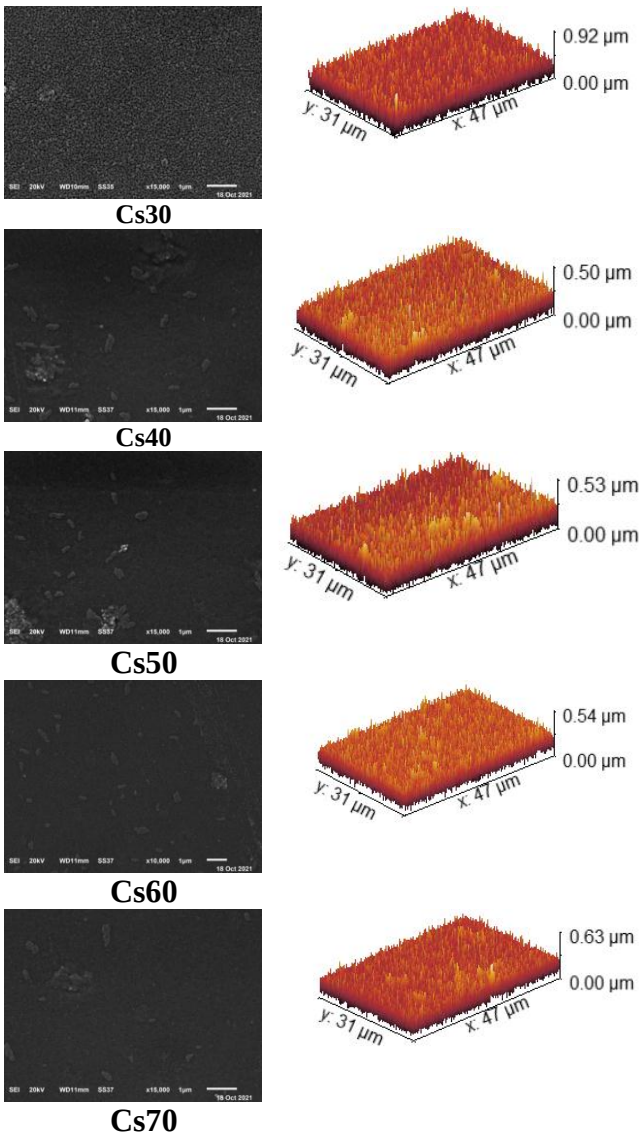

Figure (7) SEM image and their corresponding 3-dimensional (3D) images

Conclusion

Chitosan polyethylene oxide thin films with varying chitosan content were successfully prepared via the ordinary solution casting route. X-ray diffraction (XRD) pattern approves the homogeneity of all samples with varying crystallinity based on the percent of each component. The degree of crystallinity was found to be decreased with increasing chitosan content. Infrared spectral data approve the interaction between Cs and PEO through strong hydrogen bonds between hydroxyl and amino groups on chitosan molecules and ether groups in PEO. Surface morphology was observed to be sensitive to the increase in chitosan content. The increase in surface roughness combined with the increase in surface area of synthesized thin films suggested that the sample can be

used in a variety of chemical applications including heavy metal and dye adsorption.

References

1. Ahmed, H. T. & Abdullah, O. G. (2019). Preparation and composition optimization of PEO: MC polymer blend films to enhance electrical conductivity. Polymers, **11**(5), 853.
2. Kawaguchi, M. (2017). Interfacial characteristics of binary polymer blend films spread at the air-water interface. Advances in colloid and interface science, **247**, 163-171.
3. Al-Shamari, A. A., Abdelghany, A. M., Alnattar, H., & Oraby, A. H. (2021). Structural and optical properties of PEO/CMC polymer blend modified with gold nanoparticles synthesized by laser ablation in water. *Journal of Materials Research and Technology*, **12,** 1597-1605.
4. Abdelghany, A. M., Abdelrazek, E. M., Badr, S. I., & Morsi, M. A. (2016). Effect of gamma-irradiation on (PEO/PVP)/Au nanocomposite: Materials for electrochemical and optical applications. Materials & Design, 97, 532-543.
5. Abdelghany, A. M., Farea, M. O., & Oraby, A. H. (2021). Structural, optical, and electrical reinforcement of gamma-irradiated PEO/SA/Au NPs nanocomposite. *Journal of Materials Science: Materials in Electronics***, 32**, 6538-6549.
6. Hashim, A., & Habeeb, M. A. (2019). Synthesis and characterization of polymer blend-$CoFe_2O_4$ nanoparticles as a humidity sensors for different temperatures. Transactions on Electrical and Electronic Materials, **20(2)**, 107-112.
7. Zhuang, S., Cheng, R., Kang, M., & Wang, J. (2018). Kinetic and equilibrium of U (VI) adsorption onto magnetic amidoxime-functionalized chitosan beads. *Journal of Cleaner Production*, **188**, 655-661.
8. Li, J., Cai, C., Li, J., Li, J., Li, J., Sun, T., & Yu, G. (2018). Chitosan-based nanomaterials for drug delivery.*Molecules*, ***23*(10)**, 2661.
9. Kendra, D. F., & Hadwiger, L. A. (1984). Characterization of the smallest chitosan oligomer that is maximally antifungal toFusarium solani and elicits pisatin formation inPisum sativum. Experimental mycology, 8(3), 276-281.
10. Tsai, G. J., & Su, W. H. (1999). Antibacterial activity of shrimp chitosan against Escherichia coli. *Journal of food protection*, **62(3),** 239-243.
11. Jia, Z., & Xu, W. (2001). Synthesis and antibacterial activities of quaternary ammonium salt of chitosan. Carbohydrate research, **333(1),** 1-6.
12. No, H. K., Park, N. Y., Lee, S. H., & Meyers, S. P. (2002). Antibacterial activity of chitosans and chitosan oligomers with different molecular weights. *International journal of food microbiology*, **74(1-2),** 65-72.
13. Yusefi, M., Shameli, K., Lee-Kiun, M. S., Teow, S. Y., Moeini, H., Ali, R. R., ... & Abdullah, N. H. (2023). Chitosan coated magnetic cellulose nanowhisker as a drug delivery system for potential colorectal cancer treatment. *International Journal of Biological Macromolecules*, 123388.
14. Chandy, T., & Sharma, C. P. (1993). Preparation and performance of chitosan encapsulated activated charcoal (ACCB) adsorbents for small molecules. *Journal of microencapsulation*, **10(4),** 475-486.
15. Bumgardner, J. D., Wiser, R., Gerard, P. D., Bergin, P., Chestnutt, B., Marini, M., & Gilbert, J. A. (2003). Chitosan: potential use as a bioactive coating for orthopaedic and craniofacial/dental implants. *Journal of Biomaterials Science, Polymer Edition*, **14(5),** 423-438.
16. Upadhayay, P., Pal, P., Zhang, D., & Pal, A. (2023). Sea Shell Extracted Chitosan Composites and Their Applications. *Composites from the Aquatic Environment*, 293-314.
17. ur Rehman, M. S., Raza, Z. A., Rehan, Z. A., Bakhtiyar, M. J., Sharif, F., & Yousaf, M. (2023). Citric acid crosslinked biocompatible silk fibroin-mediated porous chitosan films for sustained drug release application. *Materials Today Communications*, 105373.
18. Yu, C., Wang, S., Lai, W. F., & Zhang, D. (2023). The Progress of Chitosan-Based Nanoparticles for Intravesical Bladder

Cancer Treatment. *Pharmaceutics*, **15(1),** 211.
19. Hirano, S., N.Y. Yasuharu, J. Kinugawa, H. Higashijima and T. Hayashi, 1987. Chitin and Chitosan for use as a Novel Biomedical Material. In: Advances in Biomedical Polymers (Ed. C.G. Gebelain) pp: 285-297. Plenum Press, New York.
20. Quresihi, M.T., H.S. Blair and S.J. Allen, 1992. Studies on modified chitosan membranes II: Dialysis of low molecular weight metabolites. *J. Appl. Polymer. Sci*., **46**: 263-269.
21. Mallete, W.G., H. Quigley, R.D. Gaines, N.D. Johnson. and G. Rainer, 1983. Chitosan: A new hemostatic. Ann. Thorac. Surg., **36:** 55-58.
22. Aliabadi, M., Irani, M., Ismaeili, J., Piri, H., & Parnian, M. J. (2013). Electrospun nanofiber membrane of PEO/Chitosan for the adsorption of nickel, cadmium, lead and copper ions from aqueous solution. *Chemical engineering journal*, **220**, 237-243.
23. Haider, S., & Park, S. Y. (2009). Preparation of the electrospun chitosan nanofibers and their applications to the adsorption of Cu (II) and Pb (II) ions from an aqueous solution. *Journal of Membrane Science*, **328**(1-2), 90-96.
24. Aziz, S. B., Marif, R. B., Brza, M. A., Hassan, A. N., Ahmad, H. A., Faidhalla, Y. A., & Kadir, M. F. Z. (2019). Structural, thermal, morphological and optical properties of PEO filled with biosynthesized Ag nanoparticles: New insights to band gap study. *Results in Physics*, *13*, 102220.
25. Hameed, S. T., Qahtan, T. F., Abdelghany, A. M., & Oraby, A. H. (2023). ZnO/CuO nanocomposite-based carboxymethyl cellulose/polyethylene oxide polymer electrolytes for energy storage applications. *Journal of Materials Research and Technology*, ***22***, 531-540.
26. Abdelghany, A. M., Menazea, A. A., & Ismail, A. M. (2019). Synthesis, characterization and antimicrobial activity of Chitosan/Polyvinyl Alcohol blend doped with Hibiscus Sabdariffa L. extract. *Journal of Molecular Structure*, **1197,** 603-609.
27. Asad, M., Arshad, M. N., Asiri, A. M., Rahman, M. M., Kumaran, S., & Thorakkattil Neerankuzhiyil, M. M. (2023). Chitosan–Cu Catalyzed Novel Ferrocenated Spiropyrrolidines: Green Synthesis, Single Crystal X-ray Diffraction, Hirshfeld Surface and Antibacterial Studies. *Polymers*, *15*(2), 429.
28. Pakravan, M., Heuzey, M. C., & Ajji, A. (2011). A fundamental study of chitosan/PEO electrospinning. *Polymer*, *52*(21), 4813-4824.
29. Kumar, M. R., Muzzarelli, R., Muzzarelli, C., Sashiwa, H., & Domb, A. J. (2004). Chitosan chemistry and pharmaceutical perspectives. *Chemical reviews*, *104*(12), 6017-6084.
30. Archana, D., Singh, B. K., Dutta, J., & Dutta, P. K. (2013). In vivo evaluation of chitosan–PVP–titanium dioxide nanocomposite as wound dressing material. *Carbohydrate polymers*, ***95*(1),** 530-539.
31. Al-Bataineh, Q. M., Ahmad, A. A., Alsaad, A. M., Migdadi, A. B., & Telfah, A. (2022). Correlation of electrical, thermal, and crystal parameters of complex composite films based on polyethylene oxide (PEO) doped by copper sulfate (CuSO4). *Physica B: Condensed Matter*, *645*, 414224.
32. Alsaad, A. M., Aljarrah, I. A., Ahmad, A. A., Al-Bataineh, Q. M., Shariah, A., Al-Akhras, M. A., & Telfah, A. D. (2022). The structural, optical, thermal, and electrical properties of synthesized PEO/GO thin films. *Applied Physics A*, ***128*(8),** 676.